Alteration of Imidazole Dimer on Oxidation or Water Ligation

Shihai Yan[†] and Yuxiang Bu*[,†,‡]

Key Laboratory of Colloid and Interface Chemistry of the Ministry of Education, Institute of Theoretical Chemistry, Shandong University, Jinan, 250100, P. R. China, and Department of Chemistry, Qufu Normal University, Qufu, 273165, P. R. China

Received: May 19, 2004; In Final Form: July 3, 2004

Geometry optimizations demonstrate that the proton (H_9) transfers spontaneously on oxidation by electron detachment from HOMO just for the single H-bond (N−H···N) coupling mode complexes, **NA** and **NB**, and the intrinsic mechanism of this proton transfer is presented. The absence of the imaginary frequencies for the DFT (UB3LYP/6-311+G*) structures shows that these complexes present indeed the local minima on the energy surface. Significant bond length changes for those in bonding or antibonding regions on oxidation are found with the HOMO analyses for all of these five complexes, and water ligation does not significantly affect the complex geometries. The frequency analyses indicate that a distinct red-shift occurs for the N−H···N stretching vibration of the single H-bond coupling mode complexes on oxidation and a slight blue-shift occurs for the C−H···N stretching vibration of the double H-bond coupling mode complexes on oxidation. The difference of the N−H···O and O−H···N H-bonds is compared. Both the oxidation and the water ligation increase the *Es*, leading to the strengthening of the combination of two moieties of each isomer. The coupling mode gives more contribution to *Es* as compared to the orientation, and the oxidation effect is significantly larger than the water ligation effect on the complex structures.

1. Introduction

The hydrogen-bonding interaction of two heterocyclic systems occurs in various biological complexes and is one of the most important factors determining the biological functions of these complexes.[1] This kind of intramolecular and intermolecular hydrogen bonding plays an important role in molecular conformation, crystal packing, protein folding, and the binding between some nucleoside bases.[2−9] More generally, the ordered structures of biological macromolecules are determined by a variety of intermolecular interactions in which hydrogen bonding is essential.[10] Another significant aspect is that the proton transfer can occur along hydrogen-bonded biomolecules. This transfer is thought to be as important as electron transfer for energy transduction in some biological processes. Many important investigations have reported that the organic solids with hydrogen bonds (or bridges) also have higher conductivity. It appeared that imidazole would be a good case for more detailed study.

The use of imidazole (Im) and their derivatives in chemical processes is becoming increasingly important. The possibility of its hydrogen bond formation is widely used in pharmaceuticals. Im and its derivatives form a variety of nucleophilic and general base catalysts.[11−12] The Im ring is a model molecule for more complicated systems, and is of particular interest in biology, where it is involved in nucleic acid bases and amino acids. The Im is of importance in biological systems, especially in enzyme action and protein structural determination.[13−15] In some active sites of enzymes, imidazole acts as a metabolic function. The unique ring structure of Im permits the proton to be picked up by one N atom and the other H/H^+ to be released from the other N atom. This action has been proposed to explain the proton conductivity properties[16] of Im in the solid state and also in the actual biological surrounding where a long H-bonded chain is present. Many investigations have been carried out in both experimental[16−21] and theoretical[22−27] fields regarding the properties of imidazole and its ramifications in recent years. In the experiment fields, crystalline Im has been studied for its vibrations and intra- and intermolecular force constants.[18,20] High-pressure infrared spectroscopy is used in probing the C−H···O interactions in the aqueous protonated Im.[21] In the theoretical aspect, the cation binding effect on hydrogen bonding has been explored,[22] and the Im has also been used as a model for theoretical study on the tyrosine−histidine system.[23] Some low-lying electronic states of Im and the proton-transfer shuttling with stationary and mobile Im have been investigated in detail.[24,25] The interactions of Im with other biological systems have also been carried out.[1,26]

The studies of the interaction of the imidazole molecule might provide nonnegligible contributions to the protein structure and the enzyme mechanisms in biological systems. Four intriguing coupling modes have been found in our previous investigation,[28] and they are classified as: (1) C···N mode, (2) N···N mode, (3) single H-bond, and (4) double H-bond mode.

It has been pointed out[29] that oxidative damage to DNA plays a key role in mutagenesis and carcinogenesis, which has attracted considerable interest recently.[30,31] It is well known that the imidazole ring is an essential constituent of many biological compounds such as adenine, guanine, histamine, and the histidine residues of proteins. Therefore, the generation of the ionized Im cation radical is more possible in the oxidative damage processes. In particular, a recent photodegradation mechanism investigation regarding the histidine residues in two proteins, Cu/Zn-superoxide dismutase and the CO adduct of hemoglobin, indicated that the Im^+ cation radical may be

* Corresponding author. Phone: 86-531-8365740. Fax: 86-531-8564464. E-mail: byx@sdu.edu.cn.
† Shandong University.
‡ Qufu Normal University.

10.1021/jp047828i CCC: $27.50
Published on Web 08/14/2004

produced upon photoexcitation from an initially excited state, and its more possible succeeding reactions are predicted to deprotonate and dimerize or react with other Im molecules.[32] However, the detailed coupling modes and reaction mechanism have not been explored. On the other hand, water is also one of the abundant components in the proteins, and also the strong coupling interaction with biological molecular fragments exists undoubtedly. Preliminary investigation indicates that, in the presence of one water molecule, two possible hydrogen bonds may be formed, N−H···OH_2 and N···H−OH, and some intriguing phenomena are observed.[33] Yet no investigations have been published about the oxidation and the complexation with a single water molecule upon the Im dimer. Therefore, the purpose of the present paper is to examine whether there are similar coupling modes for the imidazole dimer ($(Im)_2$) or not, and another intention is to inspect the effect of the oxidation and the water attachment on the properties of the $(Im)_2$. Obviously, the adiabatic ionization potential (AIP) is fundamental in assessing the electron-donating and -accepting ability and plays a key role in the electron-transfer process occurring in the gas phase or in the condensed phase.[34−35]

The value of the present work lies in that it is very common for the organic molecule or biological macromolecule to be oxidized or to be integrated with water in the air, and it is useful to understand this problem from the theoretical level for the practice.

2. Computational Details

The hybrid density functional methods have been successfully used in the electronic structure determinations; especially, they are uniquely successful in describing large free radicals and intermolecular complexes.[36] The reliability of the B3LYP/6-311+G* basis set level for the imidazole system has also been verified in previous papers.[28] Therefore, the $(Im)_2$ geometry is optimized using the UB3LYP method with a 6-311+G* basis set. Vibrational frequency analysis for each configuration is performed at the same level to verify whether the optimized structures correspond to true local minima in the global potential energy surface (PES). The geometry optimization has also been carried out for the hydrated neutral imidazole dimer ($(Im)_2H_2O$). The relevant properties of $(Im)_2H_2O$ are compared to those of $(Im)_2$. It has been noted that oxidation of the complexes occurs by electron detachment from the highest occupied molecular orbital (HOMO) of the neutral complex.[37] Any bond length changes should therefore reflect the electron density pattern of this orbital, with those bonds in bonding regions being weakened and lengthened, while those corresponding to antibonding regions should be strengthened and therefore shortened. For nonbonding regions, no significant bond-order changes are expected to occur on oxidation. Therefore, the HOMO orbitals of the $(Im)_2$, $(Im)_2^+$, and $(Im)_2H_2O$ complexes are explored for the inspection of the electron and hydration effect on system. The stabilization energy (*Es*) is one of the fundamental characters of the system. The existence of the hydrogen bond is a common feature for the isomers studied in this paper, and the energy of the H-bond contributes significantly to the *Es*. Because the H-bond vibrational frequency is closely related to the H-bonding strength, a reflection of the H-bonding energy (E_h), it may be used as an energetic factor to imply the H-bonding energy via a transformation. Therefore, E_h and *Es* are determined for the comparison of the effect on oxidation and water ligation. It is generally accepted that failure to correct the BSSE would have resulted in erroneous conclusions; if the interaction is weak, it seems especially important to carry out the BSSE correction. Therefore, the calculation of the *Es* in this study is corrected not only with the ZPE correction, but also with the BSSE method. The *Es* values of $(Im)_2$, $(Im)_2^+$, and $(Im)_2H_2O$ and the relevant H-bonding energies are determined according to the following relationships.

$$Es((Im)_2) = 2E(Im) - E((Im)_2) + 2ZPE(Im) - ZPE((Im)_2) - \Delta E_{BSSE} \quad (1)$$

$$Es((Im)_2^+) = E(Im) + E(Im^+) - E((Im)_2^+) + ZPE(Im) + ZPE(Im^+) - ZPE((Im)_2) - \Delta E_{BSSE} \quad (2)$$

$$Es((Im)_2H_2O) = 2E(Im) + E(H_2O) - E((Im)_2H_2O) + 2ZPE(Im) + ZPE(H_2O) - ZPE((Im)_2H_2O) - \Delta E_{BSSE} \quad (3)$$

$$E_h = 2.8591 \times 10^{-3}\omega \quad (4)$$

where ω is the corresponding H-bond stretching vibrational frequency in cm^{-1}, and E_h is in kcal/mol.

In the present paper, hybrid density functional calculations (B3LYP) have been performed throughout using the Gaussian 98 program.[38]

3. Results and Discussion

On the basis of the reliable B3LYP/6-311+G* method, two kinds of coupling modes, totally five isomers, of neutral imidazole dimer complexes are found through the geometry optimizations. It should be noted that no C···N and N···N direct coupling modes are found for the neutral imidazole dimer. The optimized geometries are all collected in Figure 1. The primary H-bond and the framework geometry parameters obtained at this level are expressed in Tables 1 and 2, respectively. For the sake of the comparison, the corresponding optimized geometries and the parameters of the $(Im)_2^+$ and $(Im)_2H_2O$ complexes are also collected in Figure 1, and Tables 1 and 2, respectively. The corresponding HOMO contour plots of the $(Im)_2$, $(Im)_2^+$, and $(Im)_2H_2O$ complexes are presented at $0.02e/au^3$ isocontour values in Figure 2, which shows the major distribution of the HOMO. The Mulliken charge populations (*Q*) of the $(Im)_2$, $(Im)_2^+$, and $(Im)_2H_2O$ complexes are collected in Table 3. The harmonic vibrational IR spectra of the complexes are exhibited in Figures 3−7, respectively. The primary vibrational modes have been assigned in these figures. The stabilization energy (*Es*) and the bonding energy of the H-bond (E_h) are collected in Table 4.

3.1. Geometrical Character. The single H-bond coupling mode complexes, **NA** and **NB**, can be taken as the image isomer. Figure 1 demonstrates that one electron oxidation results in spontaneous transfer of H_9 between two Im monomers and leads to a dehydroimidazole−imidazolium ion complex (Im−H^+Im). This phenomenon has been observed[23] by O'Malley for the phenol−imidazole system, which is a model for tyrosine oxidation in oxygenic photosynthesis. Yet the proton-transfer mechanism is not clear until now. For this system, neither a non-proton-transferred form nor a transition state structure for proton transfer between Im^+ and Im could be found on the potential energy surface. Therefore, on oxidation of $(Im)_2$, the proton is transferred in a barrierless reaction path. It is well known that the dominating contribution to the stability of Im is that there is a conjugated five-centered-six-electron big π bond (Π_5^6). Yet when one electron is detached from the HOMO, six electrons are still needed for this big π bond to keep the stability of the Im ring. After the oxidation, the lone pair electrons on

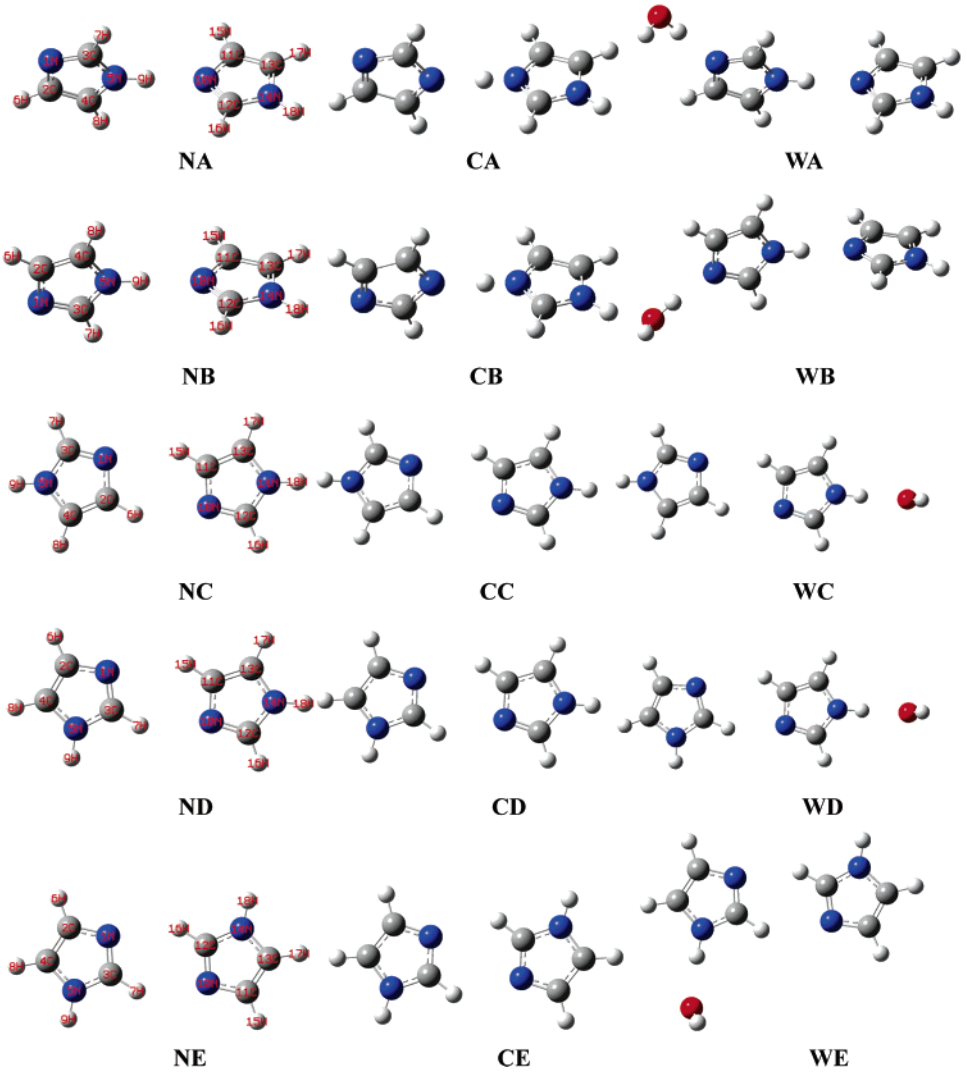

Figure 1. The optimized geometry structures of the $(Im)_2$, $(Im)_2^+$, and $(Im)_2H_2O$ complexes obtained at the B3LYP/6-311+G* level. **NX** (**X** = **A**−**E**) denotes the isomer of $(Im)_2$; **CX** denotes the isomer of $(Im)_2^+$; and **WX** denotes the isomers of $(Im)_2H_2O$. The atom serial numbers of $(Im)_2^+$ and $(Im)_2H_2O$ are similar to those of $(Im)_2$.

TABLE 1: H-Bond Parameters (*R*, Å; *A*, deg) of the $(Im)_2^+$, $(Im)_2$, $(Im)_2H_2O$, and $(Im)_2H_2O^+$ Complexes Obtained at the B3LYP/6-311+G* Basis Set Level

		$(Im)_2^+$	$(Im)_2$	$(Im)_2H_2O$			$(Im)_2^+$	$(Im)_2$	$(Im)_2H_2O$
A	R_{N-H}	1.727	1.024	1.026	D	$R_{C-H(I)}$	1.082	1.082	1.083
	$R_{H\cdots N}$	1.062	1.979	1.948		$R_{H\cdots N(II)}$	2.464	2.416	2.360
	$A_{N-H\cdots N}$	178.9	179.0	178.4		$A_{C-H\cdots N(I)}$	132.0	147.6	154.2
B	R_{N-H}	1.727	1.024	1.026		$R_{C-H(II)}$	1.081	1.081	1.081
	$R_{H\cdots N}$	1.062	1.981	1.948		$R_{H\cdots N(I)}$	2.504	2.664	2.842
	$A_{N-H\cdots N}$	179.2	178.8	178.3		$A_{C-H\cdots N(II)}$	133.1	141.1	138.3
C	$R_{C-H(I)}$	1.081	1.081	1.081	E	$R_{C-H(I)}$	1.081	1.082	1.082
	$R_{H\cdots N(II)}$	2.555	2.589	2.529		$R_{H\cdots N(II)}$	2.423	2.458	2.576
	$A_{C-H\cdots N(I)}$	134.5	146.0	150.1		$A_{C-H\cdots N(I)}$	129.3	141.5	140.0
	$R_{C-H(II)}$	1.081	1.081	1.080		$R_{C-H(II)}$	1.081	1.082	1.083
	$R_{H\cdots N(I)}$	2.555	5.588	2.694		$R_{H\cdots N(I)}$	2.423	2.464	2.389
	$A_{C-H\cdots N(II)}$	134.5	146.1	143.7		$A_{C-H\cdots N(II)}$	129.3	141.3	146.9

N_5 still participate in the reforming of the conjugated big π bond, while the odd electron on N_5 participates in the N···H−N-type H-bond for **CA** and **CB**. On the other hand, the N−H bond is broken on oxidation. Thus, the conclusion can be drawn that the electron is removed from the H_9 atom, which turns into the proton on oxidation. This proton transfer also influences the bonding character of the second moiety, although the lone pair electrons on the N_{14} atom still participate in the conjugated five-centered-six-electron big π bond (Π_5^6). The lone pair electrons on N_{10} participate in the N−H···N-type H-bond. Therefore, the attraction strength of the lone pair electrons on the N_{10} atom to H_9 should be stronger as compared to that of the odd electron on the N_5 atom, leading to the proton transfer spontaneously to the second moiety. Taking the proton transfer into consideration, the contact distance of N_5-H_9 should be increased and that of H_9-N_{10} should be decreased significantly. This can be verified by the parameters collected in Table 1. The Mulliken charge populations expressed in Table 3 can also give helpful information for the understanding of the proton transfer. The adiabatic ionization potential (AIP) calculated is

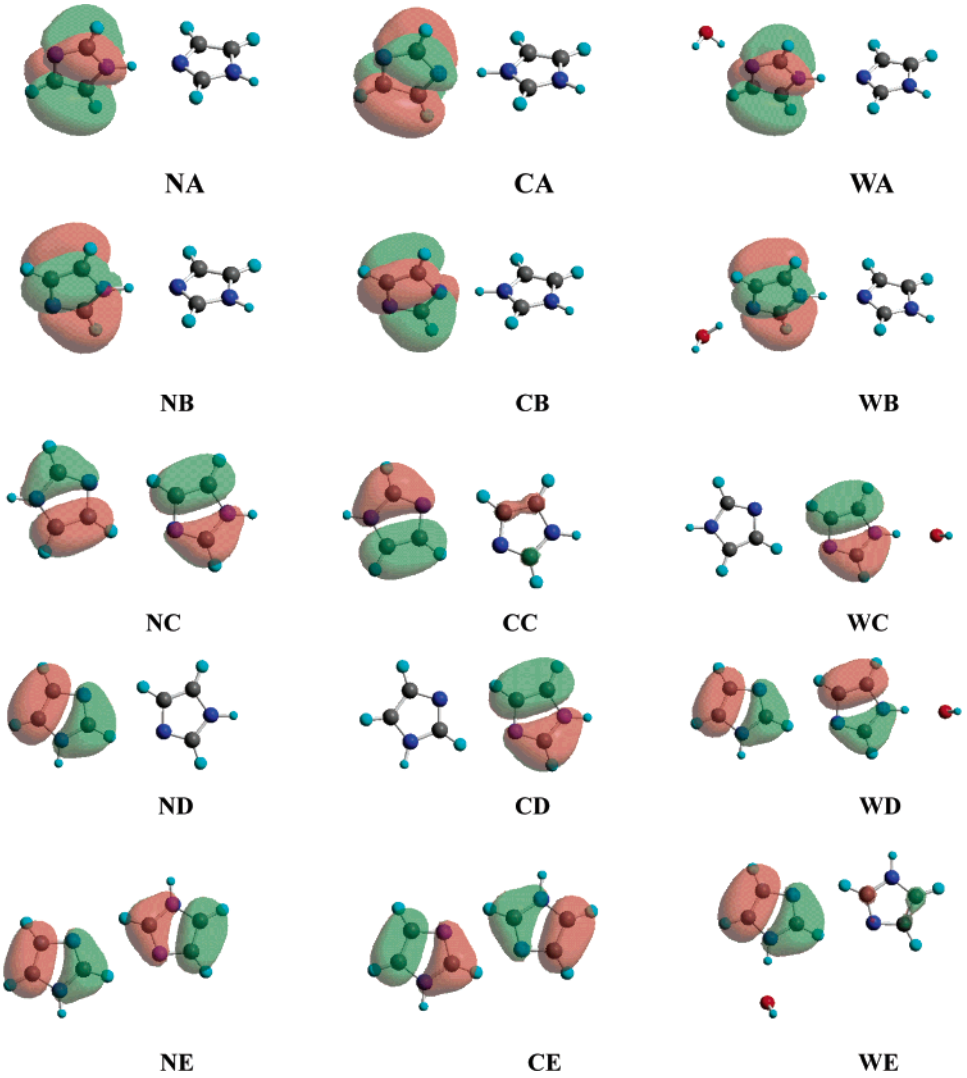

Figure 2. The HOMO of the $(Im)_2$, $(Im)_2^+$, and $(Im)_2H_2O$ complexes obtained at the UB3LYP/6-311+G* basis set level. All orbitals are contoured at 0.02 e/au^3.

TABLE 2: Selected Optimized Bond Lengths (Å) of the $(Im)_2^+$, $(Im)_2$, $(Im)_2H_2O$, and $(Im)_2H_2O^+$ Complexes Obtained at the B3LYP/6-311+G* Level

complex	isomer	N_1-C_2	N_1-C_3	C_2-C_4	C_3-N_5	C_4-N_5	$N_{10}-C_{11}$	$N_{10}-C_{12}$	$C_{11}-C_{13}$	$C_{12}-N_{14}$	$C_{13}-N_{14}$
	CA	1.319	1.357	1.469	1.381	1.325	1.380	1.329	1.361	1.339	1.382
	CB	1.319	1.356	1.469	1.382	1.325	1.380	1.329	1.361	1.339	1.382
$(Im)_2^+$	CC	1.354	1.323	1.411	1.376	1.355	1.354	1.323	1.411	1.376	1.355
	CD	1.348	1.330	1.412	1.374	1.356	1.358	1.321	1.408	1.376	1.355
	CE	1.349	1.332	1.409	1.372	1.358	1.349	1.332	1.409	1.372	1.358
	NA	1.376	1.317	1.373	1.362	1.377	1.379	1.315	1.368	1.361	1.380
	NB	1.376	1.317	1.373	1.362	1.377	1.379	1.315	1.368	1.361	1.380
$(Im)_2$	NC	1.380	1.313	1.370	1.366	1.382	1.380	1.313	1.370	1.366	1.382
	ND	1.378	1.315	1.370	1.366	1.381	1.381	1.313	1.369	1.365	1.381
	NE	1.378	1.316	1.370	1.365	1.381	1.378	1.316	1.370	1.365	1.381
	WA	1.377	1.319	1.371	1.357	1.377	1.379	1.316	1.368	1.361	1.380
	WB	1.377	1.319	1.371	1.358	1.377	1.379	1.316	1.368	1.361	1.380
$(Im)_2H_2O$	WC	1.381	1.312	1.370	1.366	1.382	1.379	1.316	1.371	1.362	1.379
	WD	1.378	1.316	1.370	1.366	1.381	1.379	1.317	1.371	1.361	1.378
	WE	1.377	1.319	1.372	1.361	1.378	1.378	1.316	1.370	1.365	1.381

~172.4 kcal/mol for **NA** and **NB**. The AIP of isolated Im determined at the same basis set level is 201.1 kcal/mol. This suggests that on hydrogen bond formation with the other Im, the AIP of Im goes down by ~30 kcal/mol. It also can be expected that the AIP can be further lowered following the elongation of the imidazole chain. Therefore, a longer imidazole chain is more favorable of the electron conductivity as compared to the short chain. Comparing the AIP of water (~290.9 kcal/mol) obtained at the same level, it can be determined that the conductivity of the imidazole chain is stronger than that of water. This is in accordance with the experimental phenomenon[16] that high conductivity in liquid imidazole is found.

The electrons occupied on the HOMO of **NA** and **NB** locate completely on the first moiety as demonstrated in Figure 2. Figure 2 also demonstrates that the oxidation of **NA** and **NB** leads to a bond elongation for the N_1-C_3, C_3-N_5, and C_2-C_4 bonds, whereas the N_1-C_2 and C_4-N_5 bonds decrease, reflecting the HOMO bonding nature of the N_1-C_3, C_3-N_5, and C_2-

TABLE 3: The Mulliken Charge Populations (*Q*) of the $(Im)_2^+$, $(Im)_2$, and $(Im)_2H_2O$ Complexes Determined at the B3LYP/6-311+G* Level

	$(Im)_2^+$					$(Im)_2$					$(Im)_2H_2O$				
	CA	CB	CC	CD	CE	NA	NB	NC	ND	NE	WA	WB	WC	WD	WE
N_1	−0.050	−0.051	−0.111	−0.068	−0.094	−0.153	−0.153	−0.152	−0.137	−0.143	−0.334	−0.337	−0.151	−0.143	−0.132
C_2	−0.145	−0.146	0.139	−0.115	−0.112	−0.237	−0.237	0.035	−0.186	−0.191	−0.198	−0.197	−0.035	−0.177	−0.220
C_3	−0.189	−0.188	−0.096	−0.152	−0.180	−0.213	−0.210	−0.152	−0.219	−0.233	−0.182	−0.181	−0.149	−0.235	−0.260
H_6	0.278	0.278	0.321	0.274	0.271	0.207	0.207	0.298	0.207	0.208	0.214	0.214	0.313	0.205	0.200
H_7	0.263	0.263	0.277	0.311	0.316	0.207	0.207	0.212	0.292	0.288	0.222	0.222	0.210	0.314	0.269
H_9	0.672	0.672	0.457	0.458	0.461	0.609	0.609	0.403	0.398	0.405	0.626	0.626	0.404	0.394	0.623
N_{10}	−0.389	−0.389	−0.111	−0.131	−0.094	−0.262	−0.260	−0.152	−0.164	−0.143	−0.255	−0.255	−0.151	−0.169	−0.149
C_{11}	−0.130	−0.132	0.139	0.124	−0.112	−0.127	−0.131	0.034	0.051	−0.191	−0.127	−0.127	0.038	0.037	−0.182
C_{12}	−0.079	−0.079	−0.096	−0.097	−0.180	−0.160	−0.161	−0.152	−0.143	−0.233	−0.162	−0.162	−0.155	−0.149	−0.240
H_{15}	0.289	0.289	0.321	0.324	0.271	0.232	0.231	0.298	0.291	0.208	0.233	0.233	0.281	0.273	0.205
H_{16}	0.295	0.295	0.277	0.274	0.316	0.233	0.233	0.212	0.214	0.288	0.233	0.233	0.201	0.203	0.302

TABLE 4: The E_h and *Es* Values (in kcal/mol) of the $(Im)_2^+$, $(Im)_2$, and $(Im)_2H_2O$ Complexes Determined at the B3LYP/6-311+G* Level

	$(Im)_2^+$		$(Im)_2$		$(Im)_2H_2O$	
	Es	E_h	Es	E_h	Es	E_h
A	35.6	7.8	7.31	9.6	13.69	9.5
B	35.6	7.8	7.31	9.6	13.68	9.5
C	21.8	9.3	1.07	9.3	5.42	9.2
		9.3		9.3		9.3
D	22.2	9.3	2.26	9.2	6.92	9.2
		9.3		9.3		9.3
E	22.9	9.3	3.47	9.2	7.83	9.2
		9.3		9.2		9.2

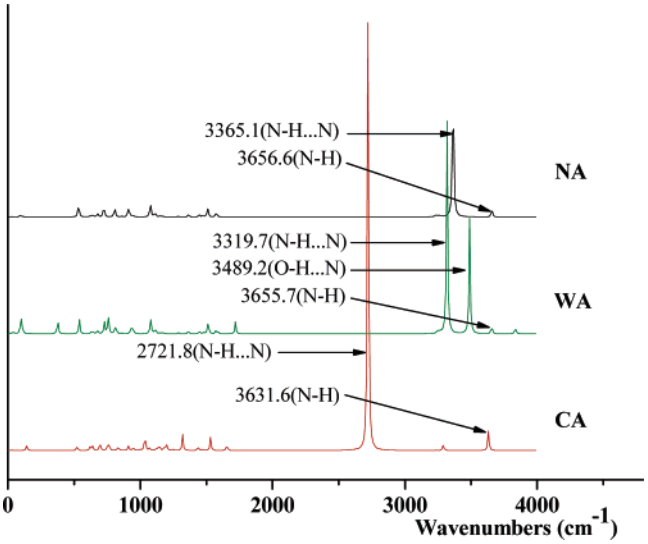

Figure 3. IR spectra of **NA**, **CA**, and **WA** obtained at the B3LYP/6-311+G* level.

C_4 bonds and the antibonding nature of the corresponding N_1-C_2 and C_4-N_5 bonds, which can be verified by the parameters expressed in Table 2. It can be calculated that the N_1-C_3, C_3-N_5, and C_2-C_4 bonds are lengthened by ∼0.04, 0.02, and 0.096 Å, respectively, while the N_1-C_2 and C_4-N_5 bonds are shortened by ∼0.057 and 0.052 Å, respectively. Significant bond length changes occur also for the $N_{10}-C_{12}$ and $C_{12}-N_{14}$ bonds. Yet these bonds belong to the second moiety, which is in the nonbonding region; therefore, these bond length alterations cannot be explained on the basis of the neutral HOMO. The most distinct contribution should be the participation of the lone pair electrons on N_{10} in the N−H···N-type H-bond. This participation leads to a lengthening of the $N_{10}-C_{12}$ bond by 0.014 Å, and a shortening of the $C_{12}-N_{14}$ bond by 0.022 Å.

The other three complexes, **NC**, **ND**, and **NE**, belong to the double H-bond coupling mode. The HOMO contour plots of these three complexes are also depicted in Figure 2, respectively. For these complexes, the lone pair electrons on the N_1 and N_{10} atoms participate in the formation of the C−H···N bonds. For **NC**, it can be seen from Figure 2 that the lone pair electrons on HOMO distribute equally on two moieties. Oxidation occurs by the electron detachment from the HOMO orbital and leads to the bond length increases for the N_1-C_3, C_3-N_5, and

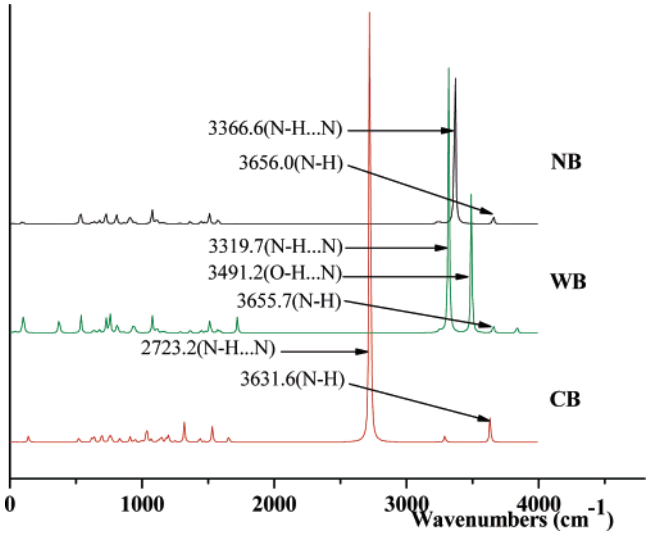

Figure 4. IR spectra of **NB**, **CB**, and **WB** obtained at the B3LYP/6-311+G* level.

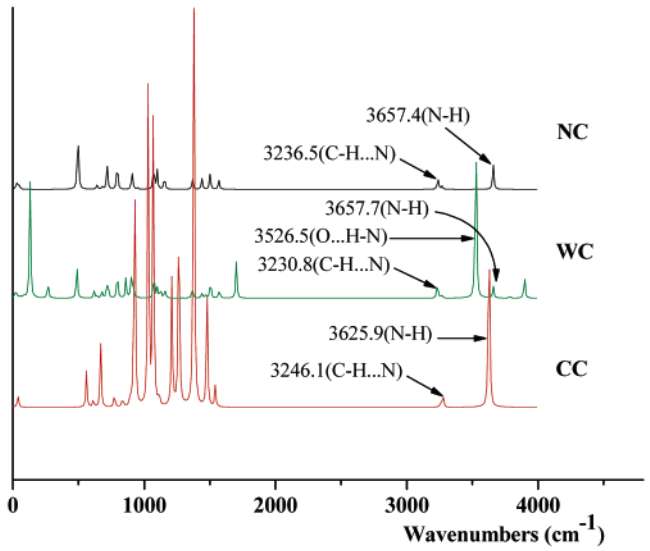

Figure 5. IR spectra of **NC**, **CC**, and **WC** obtained at the B3LYP/6-311+G* level.

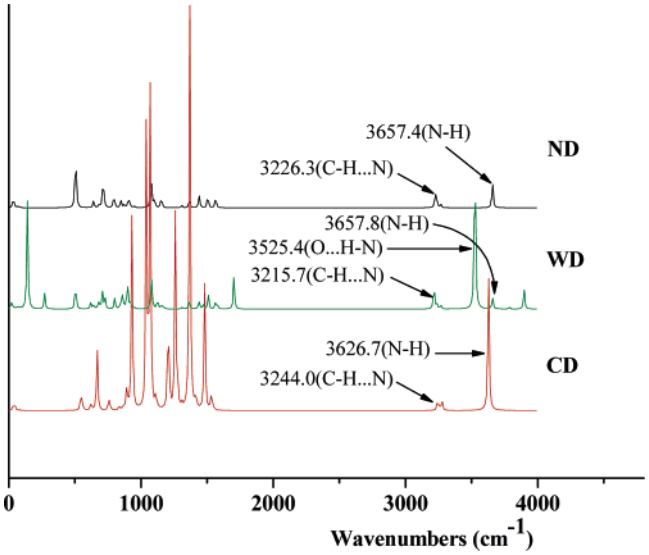

Figure 6. IR spectra of **ND**, **CD**, and **WD** obtained at the B3LYP/6-311+G* level.

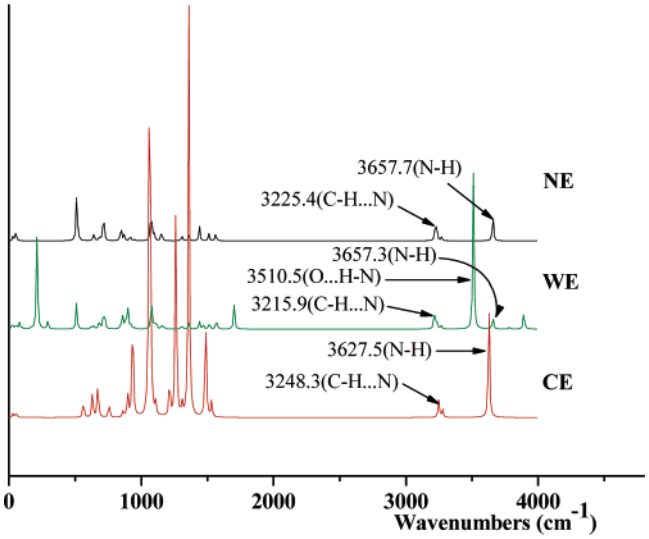

Figure 7. IR spectra of **NE**, **CE**, and **WE** obtained at the B3LYP/6-311+G* level.

C_2-C_4 bonds, whereas N_1-C_2 and C_4-N_5 decrease, reflecting the bonding HOMO nature of the former three bonds and the antibonding nature of the latter two bonds. For the $N_{10}-C_{12}$, $C_{11}-C_{13}$, $C_{12}-N_{14}$, $N_{10}-C_{11}$, and $C_{13}-N_{14}$ bonds, significant bond length changes also occur. Here again, the bonding nature of the HOMO for the $N_{10}-C_{12}$, $C_{11}-C_{13}$, and $C_{12}-N_{14}$ bonds leads to an elongation on oxidation, while the antibonding nature of the $N_{10}-C_{11}$ and $C_{13}-N_{14}$ bonds leads to a contraction on oxidation. The bond lengths expressed in Table 2 are in favor of these analyses. For **ND**, the lone pair HOMO electrons distribute on the first moiety; therefore, the changes on oxidation by the electron detachment from the HOMO orbital of this moiety should be obvious. Similarly, the elongation of the N_1-C_3, C_3-N_5, and C_2-C_4 bonds reflect the bonding nature of the HOMO, while the antibonding nature of the N_1-C_2 and C_4-N_5 leads to the contraction of both bonds on oxidation. For **NE**, the HOMO plot is similar to that of **NC**; therefore, the bond length changes of **NE** have tendencies similar to those of **NC**. This can be verified by the data summarized in Table 2. It can be also seen from this table that the contact distances (H-bond) of two moieties of NC are shortened on oxidation, while this shortening of the contact distances of two moieties is just in accordance with the antibonding nature of HOMO between two moieties shown in Figure 2. A similar phenomenon can be observed for NE when it is oxidized. The conversion of C_3-H_7 from the bonding HOMO nature in **ND** to the nonbonding HOMO nature leads to the lengthening of H···N from 2.416 to 2.464 Å. On the contrary, the alternation of $C_{11}-H_{15}$ from the nonbonding HOMO nature in **ND** to the bonding HOMO nature leads to significant shortening of H···N from 2.664 to 2.504 Å. Another point that should be noted is that not only are two moieties in symmetry, but also the changes of two moieties on oxidation are in symmetry for **NC** and **NE**. The AIPs of these three complexes are also determined at same basis set level to be 180.3, 181.0, and 181.5 kcal/mol, respectively, ~10 kcal/mol higher than those of the single H-bond coupling mode complexes, while they are ~20 kcal/mol lower as compared to the AIP of Im monomer. Therefore, the conclusion can be drawn that the double H-bond coupling mode complexes are more difficult to be ionized as compared to the single H-bond mode complexes.

On the basis of the optimized $(Im)_2$ geometry, one water is attached to the N position and forming new O−H···N or O···H−N-type H-bond. For the single H-bond coupling mode (**NA** and **NB**), the O−H group of the water participates in the H-bond and forming O−H···N-type H-bond, in which the lone pair electrons of N are shared with the O−H group, while for the double H-bond coupling mode (**NC**, **ND**, and **NE**), the O atom participates in the formation of the O···H−N-type H-bond, in which the lone pair electrons of O are shared with the N−H group. Obviously, the chief distinction of the O−H···N- and O···H−N-type H-bonds is which lone pair electrons participate in the H-bond formation.

For the complexes involving the O−H···N-type H-bond, **WA** and **WB**, the O−H group interacts with the N_1 atom. From Figure 2, it can be seen that the HOMO orbitals of **WA** and **WB** are similar to those of **NA** and **NB**. The participation of the lone pair electrons on N_1 atom in the H-bond formation leads to the weakening of the interaction between N_1-C_2 and N_1-C_3; therefore, these two bond lengths should be lengthened. This also can be reflected from the charge distributions expressed in Table 3. Comparing the charge distributions before and after water ligation, one can see clearly that the negative charge at the N_1 atom position increases significantly while the influence on the C_2 and C_3 positions is weak. The antibonding HOMO nature of the N_1-C_2 bond and the bonding nature of the HOMO of the N_1-C_3 bond have been demonstrated in former analyses, and it is well known that the increasing of the electrons will lead to not only the bond lengthening for the bonds distributed in the antibonding region, but also the bond shortening for those distributed in the bonding region. Therefore, the elongation of N_1-C_2 and the shortening of N_1-C_3 are reasonable. The polarity of the $(Im)_2$ is strengthened when the $(Im)_2H_2O$ complex is formed with the ligation of the water. This can be illuminated with their dipole moments, those of **WA** and **WB** (~11.6 D) are obviously bigger as compared to those of **NA** and **NB** (~9.3 D). The contact distance of N···H decreases from ~1.98 to ~1.95 Å, so the combination of two Im moieties should be strengthened on water ligation, leading to the contraction of two molecular fragments. Therefore, the conclusion can be drawn with the reference of the bond parameters expressed in Tables 1 and 2 that the effect brought by the water attachment is weaker as compared to that caused by oxidation on **NA** and **NB**.

Tables 1 and 2 also demonstrate that the ligation of water has no significant influence on the bond length changes for the

double H-bond coupling mode complexes. For the complexes **WC**, **WD**, and **WE**, the O atom interacts with the N−H group, forming the O···H−N-type H-bond. The ligation of water not only breaks out the symmetry, but also increases the polarity of the complexes. Their dipole moments increase to 3.5, 6.7, and 2.8 D from 0.0, 3.3, and 0.0 D of **NC**, **ND**, and **NE**, respectively. Therefore, the bond length changes occur mainly on the contact distance of two moieties and the bond lengths of the moiety and the water attached, although the changes are not notable. Also one H-bond is expected to be strengthened and shortened, while the other one is expected to be weakened and lengthened. For **NC** and **ND**, the bond length changes are expected to occur on the second moiety on the ligation of water, while the changes of **NE** are expected to occur on the first moiety. The bond parameters expressed in Tables 1 and 2 can illustrate this conclusion very well.

3.2. Frequency Analyses. The absences of imaginary frequencies for the B3LYP/6-311+G* geometry structures show that these five isomers (**NA**−**NE**) present indeed the local minimum on the energy surface, respectively. Similarly, the calculated harmonic vibrational frequencies of the corresponding $(Im)_2^+$ and $(Im)_2H_2O$ complexes also demonstrate that they are really stable structures. The harmonic vibrational IR spectra of these complexes are exhibited in Figures 3−7, respectively. The primary vibrational modes are also assigned in these figures. Here, the emphasis of the present paper is to investigate the alterations of the vibrational frequencies on oxidation and on water ligation. One common characteristic can be seen from these figures: the vibrational frequencies of these complexes with notable IR intensities densely distribute in the fingerprint section. This observation is in good accordance with the results obtained in a previous study.[28]

Figures 3 and 4 demonstrate that the vibrational frequency of the N−H···N stretching mode is red-shifted distinctly on oxidation for the single H-bond coupling mode complexes (**NA** and **NB**) of $(Im)_2$ by ∼640 cm^{-1}. From the above analyses, it is clear that the dominant contribution should be the electron detachment from the H_9 atom on oxidation. Therefore, the electron density between two nitrogen atoms decreases significantly, leading to the decrease of the electrostatic interaction of this H-bond. The participation of the lone pair electrons on the N_{10} atom also decreases the electron density of the second moiety; therefore, the $N_{14}-H_{18}$ stretching mode is red-shifted. From Figures 3 and 4, it is clear that the N−H···N stretching mode of **NA** and **NB** is also red-shifted on water ligation by ∼45 cm^{-1}. The prominent contribution to this red-shift should be the decreasing of the electron density among the first moiety on the water ligation. Yet the effect of this ligation on the second moiety of **NA** and **NB** is weak; therefore, the changes of the vibrational frequencies of the second moiety are illegible. Another point also should be noted with reference to Figures 3 and 4, that on water attachment one new O−H···N-type H-bond is formed, and this H-bond also carries notable IR intensity.

Figures 5−7 display the IR spectra of **NC**, **ND**, and **NE** obtained at the B3LYP/6-311+G* level. For the convenience of comparison, the corresponding IR spectra of **CC** and **WC**, **CD** and **WD**, and **CE** and **WE** are also collected in Figures 5−7, respectively. One common characteristic of these three double H-bond coupling mode complexes is that there are several harmonic frequencies distributed among the fingerprint section, which carries notable IR intensity on oxidation, and these frequencies of $(Im)_2^+$ have been discussed in our previous paper;[28] therefore, our emphasis is placed on the alterations of the frequencies from $(Im)_2$ to $(Im)_2^+$ and $(Im)_2H_2O$. It is generally accepted that the electron density decreases on oxidation, and the vibrational frequencies are red-shifted for the weakening of the interaction. For example, the N−H stretching modes expressed in Figures 5−7 are red-shifted by 31.5, 30.7, and 30.2 cm^{-1} for **NC**, **ND**, and **NE**, respectively. It seems illogical for the blue-shift of the C−H···N stretching mode on oxidation by 9.6, 17.7, and 22.9 cm^{-1}, respectively. With the above analyses about the geometry, the conclusion has been drawn that the C−H···N H-bonds of **NC**, **ND**, and **NE** are shortened and their attractions have been strengthened. Therefore, the blue-shift of the corresponding vibrational frequency is reasonable. It is the O atom instead of the O−H group of water that participates in the formation of the new O···H−N-type H-bond. The effect on the electron density of $(Im)_2$ should be smaller as compared to that caused by O−H···N-type H-bond, although both of their functions are to decrease the electron density of the system. The vibrational frequencies expressed in Figures 3−7 can illustrate this conclusion. The frequency of the C−H···N stretching mode is red-shifted by ∼10 cm^{-1} on water ligation. The effect on the N−H stretching mode is weak.

3.3. Stabilization Energy. The calculated stabilization energies, *Es*, of the $(Im)_2^+$, $(Im)_2$, and $(Im)_2H_2O$ complexes using the B3LYP method employing the 6-311+G* basis set are collected in Table 4. The corresponding bonding energy of the H-bond (E_h) also is represented in this table.

From the *Es* expressed in Table 4, the following four points can be concluded. First, the order of the *Es* of $(Im)_2$ is **NA** = **NB** > **NE** > **ND** > **NC**, and the orders of $(Im)_2^+$ and $(Im)_2H_2O$ are similar to that of $(Im)_2$; in other words, the orders of $(Im)_2^+$ and $(Im)_2H_2O$ are **CA** = **CB** > **CE** > **CD** > **CC** and **WA** = **WB** > **WE** > **WD** > **WC**, respectively. This indicates that the order of *Es* of $(Im)_2$ is not changed, although the properties of the system have been altered on oxidation or on water ligation. Second, the isomers carrying the N−H···N-type H-bond are more stable as compared to those containing two C−H···N-type H-bonds of $(Im)_2$; similar phenomena are observed for the isomers of $(Im)_2^+$ and $(Im)_2H_2O$. This point can be understood from the following two aspects. One is the E_h expressed in Table 4. It can be seen that the E_h values of isomers carrying the N−H···N-type H-bond are stronger as compared to those containing the C−H···N-type H-bond for $(Im)_2$ and $(Im)_2H_2O$. For the isomers of $(Im)_2^+$, it seems reverse, but the analyses in a previous paper[28] illustrate that the proton transfer lowers the energy of the system of $(Im)_2^+$ significantly. The other aspect that is helpful for the understanding of this point is the strong repulsion brought by the coplanar arrangement of two Im fragments. This demonstrates that the attraction of two moieties of **NA** or **NB** should be stronger as compared to those of **NC**, **ND**, and **NE**. Therefore, **NA** and **NB** should be more stable as compared to **NC**, **ND**, and **NE**. It is similar for the isomers of $(Im)_2^+$ and $(Im)_2H_2O$. The third point that can be drawn from the *Es* represented in Table 4 is that there almost is no difference between two isomers of each complex with the N−H···N-type H-bond, and the difference of the other three isomers with the C−H···N-type H-bond is also indistinctive. It indicates that the contribution of the coupling mode to *Es* is more significant as compared to that of the orientation. The last one that should also be pointed out is the values of *Es* of the $(Im)_2$, $(Im)_2^+$, and $(Im)_2H_2O$ complex. The *Es* of $(Im)_2^+$ is bigger as compared to the corresponding *Es* of $(Im)_2H_2O$. Therefore, the conclusion can be drawn that the system is stabilized on oxidation and on water ligation; in other words, the combination of two moieties for each isomer of $(Im)_2^+$ and $(Im)_2H_2O$ is compact and the

complex is not as easy to decompose as $(Im)_2$. The influence of the system on oxidation is more significant as compared to that on water ligation, in accordance with the conclusion drawn from the former analyses.

4. Conclusion

The full geometry optimizations are performed for the neutral imidazole dimer $(Im)_2$ at the UB3LYP/6-311+G* basis set level. The results are compared to the corresponding optimized complexes of imidazole and imidazole cation $(Im)_2^+$. The corresponding optimized geometries of water ligated $(Im)_2$, $(Im)_2H_2O$, are also obtained at the same level.

Only single and double H-bond two-coupling modes are found on geometry optimization. The proton (H_9) transfer is spontaneous on oxidation by removing an electron from the HOMO of the single H-bond coupling mode isomers of $(Im)_2$. The intrinsic mechanism for this proton transfer mainly lies in the changes of the electron distribution on the oxidation of $(Im)_2$. It is expected that the AIP is decreased following the lengthening of the Im chain. The Mulliken charge population reflects the bond changes on oxidation and the water ligation. The analysis about HOMO also demonstrates the tendency of the alterations of the bond lengths on oxidation or water ligation. The frequency analyses indicate that a distinct red-shift occurs for the N−H···N stretching mode of the single H-bond coupling mode complexes on oxidation for the decreasing of the electron density on this H-bond. The C−H···N stretching mode of the double H-bond coupling mode complexes is blue-shifted on oxidation for the electron redistribution. The differences of the N−H···O and O−H···N-type H-bonds are compared. The effect of the O−H···N-type H-bond brought to the system is stronger as compared to that brought by the N−H···O-type H-bond. The coupling mode contributes more to *Es* than the orientation for this system. The *Es* values are increased both on oxidation and on water ligation, although the order of *Es* is not altered. The conclusion can be safely drawn that the effect brought by the water ligation is weaker as compared to that brought by the oxidation on $(Im)_2$.

Acknowledgment. This work is supported by the National Natural Science Foundation of China (20273040) and the Natural Science Foundation of Shandong Province (Key project). The support from SRFDP and the Foundation for University Key Teacher by the Ministry of Education of China is also acknowledged.

References and Notes

(1) Jalbout, A. F.; Adamowicz, L. *J. Phys. Chem. A.* **2001**, *105*, 1071.
(2) Berger, I.; Egli, M.; Rich, A. *Proc. Natl. Acad. Sci. U.S.A.* **1996**, *93*, 12116.
(3) Brandl, M.; Lindauer, K.; Meyer, M. Suhnel, J. *Theor. Chem. Acc.* **1999**, *101*, 103.
(4) Steiner, T.; Saenger, W. *J. Am. Chem. Soc.* **1992**, *114*, 10146.
(5) Takahara, P. M.; Frederick, C. A.; Lippard, S. J. *J. Am. Chem. Soc.* **1996**, *118*, 12309.
(6) Ash, E. L.; Sudmeier, J. L.; Day, R. M.; Vincent, M.; Torchilin, E. V.; Haddad, K. C.; Bradshaw, E. M.; Sanford, D. G.; Bachovchin, W. W. *Proc. Natl. Acad. Sci. U.S.A.* **2000**, *97*, 10371.
(7) Musah, R. A.; Jensen, G. M.; Rosenfeld, R. J.; McRee, D. E.; Goodin, D. B.; Bunte, S. W. *J. Am. Chem. Soc.* **1997**, *119*, 9083.
(8) Jeffrey, G. A.; Saenger, W. *Hydrogen Bonding in Biological Structures*; Springer-Verlag: New York, 1994.
(9) Wahl, M. C.; Sundaralingam, M. *Trends Biochem. Sci.* **1997**, *22*, 97.
(10) Brédas, J. L.; Poskin, M. P.; Delhalle, J.; André, J. M.; Chojnacki, H. *J. Phys. Chem.* **1984**, *88*, 5882.
(11) Bender, M. L.; Bergeron, R. J.; Komiyama, M. *The Bioorganic Chemistry of Enzymatic Catalysis*; Wiley-Interscience: New York, 1984; p 312.
(12) Stewart, P. *The Proton: Applications to Organic Chemistry*; Academic Press: Orlando, FL, 1985; Vol. 46, p 313.
(13) Bachovchin, W. W. *Biochemistry* **1986**, *25*, 7751.
(14) Noguchi, T.; Inoue, Y.; Tang, X. S. *Biochemistry* **1999**, *38*, 399.
(15) Sorlie, M.; Christiansen, J.; Lemon, B. J.; Peters, J. W.; Dean, D. R.; Hales, B. J. *Biochemistry* **2001**, *40*, 1540.
(16) Kawada, A.; McGhie, A. R.; Labes, M. M. *J. Chem. Phys.* **1970**, *52*, 3121.
(17) Perchard, C.; Novak, A. *J. Chem. Phys.* **1968**, *48*, 3079.
(18) Colombo, L.; Bleckmann, P.; Schrader, B.; Schneider, R.; Plesser, Th. *J. Chem. Phys.* **1974**, *61*, 3270.
(19) Christen, D.; Griffiths, J. *Z. Naturforsch.* **1982**, *37a*, 1378.
(20) Loeffen, P. W.; Pettifer, R. F.; Fillaux, F.; Kearley, G. J. *J. Chem. Phys.* **1995**, *103*, 8444.
(21) Su, C. C.; Chang, H. C.; Jiang, J. C.; Wei, P. Y.; Lu, L. C.; Lin, S. H. *J. Chem. Phys.* **2003**, *119*, 10753.
(22) Basch, H.; Krauss, M.; Stevens, W. J. *J. Am. Chem. Soc.* **1985**, *107*, 7267.
(23) O'Malley, P. J. *J. Am. Chem. Soc.* **1998**, *120*, 11732.
(24) Machado, F. B. C.; Davidson, E. R. *J. Chem. Phys.* **1992**, *97*, 1881.
(25) Scheiner, S.; Yi, M. Y. *J. Phys. Chem.* **1996**, *100*, 9235.
(26) Tatara, W.; Wójcik, M. J.; Lindgren, J.; Probst, M. *J. Phys. Chem. A* **2003**, *107*, 7827.
(27) Chojnacki, H.; Lipinski, J. *Adv. Mol. Relax. Interact. Processes* **1980**, *18*, 149.
(28) Yan, S. H.; Bu, Y. X.; Cao, Z. H.; Li, P. *J. Phys. Chem. A*, in press.
(29) Schumm, S.; Prévost, M.; García-Fresnadillo, D.; Lentzen, O.; Moucheron, C.; Kirsch-De Mesmaeker, A. *J. Phys. Chem. B* **2002**, *106*, 2763.
(30) (a) Pogozelski, W. K.; Tullius, T. D. *Chem. Rev.* **1998**, *98*, 1089. (b) Burrows, J. C.; Muller, J. G. *Chem. Rev.* **1998**, *98*, 1109. (c) Armitage, B. *Chem. Rev.* **1998**, *98*, 1171.
(31) (a) Saito, I.; Takayama, M.; Sugiyama, H.; Nakatami, K. *J. Am. Chem. Soc.* **1995**, *117*, 6406. (b) Sugiyama, H.; Saito, I. *J. Am. Chem. Soc.* **1996**, *118*, 7063. (c) Hutter, M.; Clark, T. *J. Am. Chem. Soc.* **1996**, *118*, 7574. (d) Steenken, S.; Jovanovic, S. *J. Am. Chem. Soc.* **1997**, *119*, 6617. (e) Prat, F.; Houk, K. N.; Foote, C. S. *J. Am. Chem. Soc.* **1998**, *120*, 845. (f) Kim, N. S.; Zhu, Q.; LeBreton, P. R. *J. Am. Chem. Soc.* **1999**, *121*, 11516. (g) Russo, N.; Toscano, M.; Grand, A. *J. Comput. Chem.* **2000**, *21*, 1243. (h) Saito, I.; Nakamura, T.; Nakatami, K. *J. Am. Chem. Soc.* **2000**, *122*, 3001.
(32) Wu, Q.; Balakrishnan, G.; Pevsner, A.; Spiro, T. G. *J. Phys. Chem. A* **2003**, *107*, 8047.
(33) Van Bael, M. K.; Smets, J.; Schoone, K.; Houben, L.; McCarthy, W.; Adamowicz, L.; Nowak, M. J.; Maes, G. *J. Phys. Chem. A* **1997**, *101*, 2397.
(34) Chen, E. S. D.; Chen, E. S. M.; Sane, N.; Shulze, S. *Bioelectrochem. Bioenerg.* **1999**, *48*, 69.
(35) Periquet, V.; Moreau, A.; Carles, S.; Schermann, J. P.; Desfrancois, C. *J. Electron. Spectrosc. Relat. Phenom.* **2000**, *106*, 141.
(36) (a) O'Malley, P. J.; Collins, S. J. *Chem. Phys. Lett.* **1996**, *259*, 296. O'Malley, P. J. *Chem. Phys. Lett.* **1996**, *262*, 797. (b) O'Malley, P. J. *J. Phys. Chem. A* **1997**, *101*, 6334; **1997**, *101*, 9813; **1998**, *102*, 248. (c) Adamo, C.; Barone, V. In *Recent Development in Density Functional Methods*; Chong, D. P., Ed.; World Scientific Publishing: Singapore, 1997; Part II. (d) Himo, F.; Graslund, A.; Eriksson, L. E. *Biophys. J.* **1997**, *72*, 1556. (e) Qin, Y.; Wheeler, R. A. *J. Chem. Phys.* **1995**, *102*, 1689.
(37) O'Malley, P. J.; Collins, S. J. *J. Am. Chem. Soc.* **2001**, *123*, 11042.
(38) Frisch, M. J.; Trucks, G. W.; Schlegel, H. B.; Scuseria, G. E.; Robb, M. A.; Cheeseman, J. R.; Zakrzewski, V. G.; Montgomery, J. A.; Stratmann, R. E., Jr.; Burant, J. C.; Dapprich, S.; Millam, J. M.; Daniels, A. D.; Kudin, K. N.; Strain, M. C.; Farkas, O.; Tomasi, J.; Barone, V.; Cossi, M.; Cammi, R.; Mennucci, B.; Pomelli, C.; Adamo, C.; Clifford, S.; Ochterski, J.; Petersson, G. A.; Ayala, P. Y.; Cui, Q.; Morokuma, K.; Malick, D. K.; Rabuck, A. D.; Raghavachari, K.; Foresman, J. B.; Cioslowski, J.; Ortiz, J. V.; Stefanov, B. B.; Liu, G.; Liashenko, A.; Piskorz, P.; Komaromi, I.; Gomperts, R.; Martin, R. L.; Fox, D. J.; Keith, T.; Al-Laham, M. A.; Peng, C. Y.; Nanayakkara, A.; Gonzalez, C.; Challacombe, M.; Gill, P. M. W.; Johnson, B.; Chen, W.; Wong, M. W.; Andres, J. L.; Gonzalez, C.; Head-Gordon, M.; Replogle, E. S.; Pople, J. A. *Gaussian 98*; Gaussian, Inc.: Pittsburgh, PA, 1998.